Circumferential confinement consequence on the magnetic properties of a punctured nanotube in the presence of an axial electric field

A Ghasemifard[ID], M Sharifian and E Faizabadi[1][ID]

School of Physics, Iran University of Science and Technology 1684613114, Tehran, Iran

E-mail: alireza_ghasemifard@physics.iust.ac.ir, m_sharifian94@physics.iust.ac.ir and edris@iust.ac.ir

Abstract

In this paper, we present magnetic properties of a finite graphene sheet with a triangle punctured vacancy, and its counterpart single-wall carbon nanotube as a rolled-up graphene sheet in the framework of the Hubbard model in the presence of an axial electric field, in order to form a comparison study between these two graphene samples. We have noticed that the tight-binding part of the Hamiltonian consists of two types of zero-energy states in the case of the graphene sheet, the strict zero-energy states, and the quasi zero-energy states. The first type takes part in a ferromagnetic coupling between the triangle edges and one edge of the rectangle graphene sheet, while the latter one has an antiferromagnetic alignment with the opposite edge of the rectangle graphene sheet. Involving the Coulomb interaction through Hubbard term, we have observed that the slope of the cluster edge states in nanotube is higher than the graphene sheet. Additionally, spin-depolarization happens in single-wall nanotube sooner than the graphene sheet by slightly increasing an axial electric field. Also, the graphene sheet is more robust than the single wall nanotube at low electric fields.

Keywords: electronic structure, magnetic properties, Hubbard model, tight-binding, graphene, carbon nanotube

(Some figures may appear in colour only in the online journal)

1. Introduction

Carbon nanomaterials reveal a rich various allotrope, which exhibits different physical properties; that is why carbon nanostructures are playing an essential role in nanoscience [1]. One of these structures is graphene that is a single layer graphite sheet with chiral vectors (n, m) consists of two sublattices (A and B) forming a honeycomb lattice. It has numerous properties such as edge effect on the zigzag graphene nanoribbons, which depends strongly on the geometry of the boundary [2–4] and magnetization in graphene nanostructures which is not a trivial property in carbon nanomaterials [5]. Particular interest is the graphene edges of a specific crystallographic

orientation comprising carbon atoms from only one sub-lattice of the bipartite hexagonal lattice are predicted to host magnetic order [6, 7]. Carbon nanotubes attracted much attention due to its possible applications for nanoscale electronic devices [8, 9] like ballistic transport [10–12], high-performance field-effect transistors [13–17] and logic devices [18–23].

A single-wall carbon nanotube is a graphene sheet rolled into a cylindrical shape. A high ratio of surface to volume of carbon nanotube is one of the most important properties of produced materials at the nanoscale, in which their bulk behavior replaces with surface one. Furthermore, magnetic properties of graphene-based nanostructures exhibit different features from ordinary graphene (which is not magnetic) due to the existence of edge states. There are three well-known

---

[1] Author to whom any correspondence must be addressed.

methods to fabricate carbon nanotubes of desired properties that are needed for a particular application, including the electric arc discharge [24, 25], UV-sensitive self-assembled photoresist [26], and the chemical self-assembly [27, 28]. In each technique, it is possible to have some vacancies in producing carbon nanotube structures. The origin of magnetism is generally attributed to atomic-scale structural defects locally breaking the sub-lattice balance of the bipartite hexagonal lattice. The imbalance of sublattice atoms leads to a band of degenerate states near the Fermi energy level, as illustrated in figures 1(c) and (d). These midgap states are localized at the zigzag edges and lead to spin polarization of the ground state, although a graphene nanostructure with zigzag edges may have either ferromagnetic or antiferromagnetic ordered ground states, while graphene nanostructures with armchair edges are always nonmagnetic. As in the zigzag case, electron–electron interactions split the zero-energy bands and give rise to edge magnetization. Both the density functional theory (DFT) calculations and the mean-field approximation of the single-band Hubbard model with first-neighbors hopping, yield very similar results in all cases considered in the literature [6, 29]. Mean-field calculations confirm that the total spin of the ground state is $S = (N_A - N_B)/2$ and almost always localized on the edges. Where N_A and N_B are the number of sites belonging to each sublattice. Thus, a defective structure can present a finite sublattice imbalance with $|N_A - N_B|$ midgap states. Importantly, the Lieb theorem [30] predicts that any imbalance between A and B sites generates ferromagnetic ordering in the ground state of the Hubbard model and bipartite lattices at half-filling. Lieb theorem provides an intensive connection between vacancies in the graphene lattice and the emergence of magnetism.

By tuning the electric field, first, we compare spin-resolved edge states and spin depolarization which strongly depend on the applied electric field and the action of rolling. Second, the evolution of total spin and variation of the HOMO–LUMO gaps of a graphene sheet and single-wall carbon nanotube. Finally, we show that the local density of electrons on the edges can be tuned by increasing the strength of the electric field and have different behavior in both structures. We applied the electric field in a way that finite graphene sample with a triangle defect and its counterpart carbon nanotube as a rolled-up graphene sheet, experience exactly, the same on-site energy condition. This identical condition leads to a comparison study between the graphene sheet and carbon nanotube and investigates the rolling action inflict negligible effect in magnetic properties. This rolling procedure does not destroy birpartitism of the graphene lattice, which means each atom in sublattice A is connected to its first-neighbors atom in sublattice B in both structures.

To the best of our knowledge, this kind of comparison between single-layer graphene sheet and single-wall carbon nanotube has not been studied yet. Since single-wall carbon nanotube is a rolled-up graphene sheet with a well-defined triangle zigzag edge, this theoretical calculation motivates our study of the magnetization because of surface or more properly edge effects.

The rest of this paper is organized as follows. In section 2, we specify the structures and review the single-orbital Hubbard model in the presence of an axial electric field. Results and discussion are presented in section 3 and give a conclusion view in section 4.

2. Structure and method

The system of interest in the present paper is focused on two types of graphene nanostructures. The first one is a single layer finite graphene sheet with a single hole drilled into the system figure 1(a). The hole is created by removing a set of atoms and built as a triangle hole with zigzag edges. The second type of structure is rolled-up mentioned graphene sheet as a single-wall carbon nanotube with the exact hole figure 1(b). Note that this hole is the reason for zigzag edge orientation in both systems. Sublattices A and B have not differed from each other in two structures. Bottom-up fabrication [31, 32] has shown that precisely controlled processes can be developed in the near future to consider such defects with clean zigzag configuration. We assume that all edge carbon atoms are passivated.

In this paper, we study the magnetic properties of a defective finite graphene sheet and its counterpart nanotube as a rolled-up graphene sheet using a combination of tight-binding Hamiltonian and one-orbital Hubbard model, which is expressed at the mean-field approximation in the presence of an axial electric field. This model considers only the π-symmetry electronic states, which are formed by unhybridized p_z atomic orbitals of sp^2 carbon atoms. We solve the Hamiltonian

$$H = H_E + H_0 + H' \tag{1}$$

The first term is due to electric field pointed along x axes and can be written as follows:

$$H_E = \sum_{i,\sigma} \epsilon_{i,\sigma} c_{i,\sigma}^{\dagger} c_{j,\sigma}, \tag{2}$$

in which the $\epsilon_i = -ex_iE$ describes the effect of the electric field. E denote the electric field strength, e is the electron charge and x_i is the position of ith carbon atom along the x-direction. Operators $c_{i,\sigma}^{\dagger}$ and $c_{i,\sigma}$ create and annihilate the electron with spin σ at site i, respectively.

The second term is the usual tight-binding Hamiltonian

$$H_0 = -t \sum_{\langle i,j \rangle, \sigma} (c_{i,\sigma}^{\dagger} c_{j,\sigma} + \text{h.c.}), \tag{3}$$

The notation $\langle i,j \rangle$ stands for pairs of first nearest-neighbors atoms and also h.c. is the Hermitian conjugate counterpart. The hopping integral between site i and j is chosen $t = -2.66$eV that defines the energy spectrum of the Hamiltonian. From the computational point of view, the off-diagonal matrix elements (i,j) and (j,i) are set to t when atoms i and j are covalently bonded, and to 0 otherwise. In addition, electron–electron interactions have to be introduced in order to describe the onset of magnetism. These interactions can be written in terms of the single-band Hubbard model:
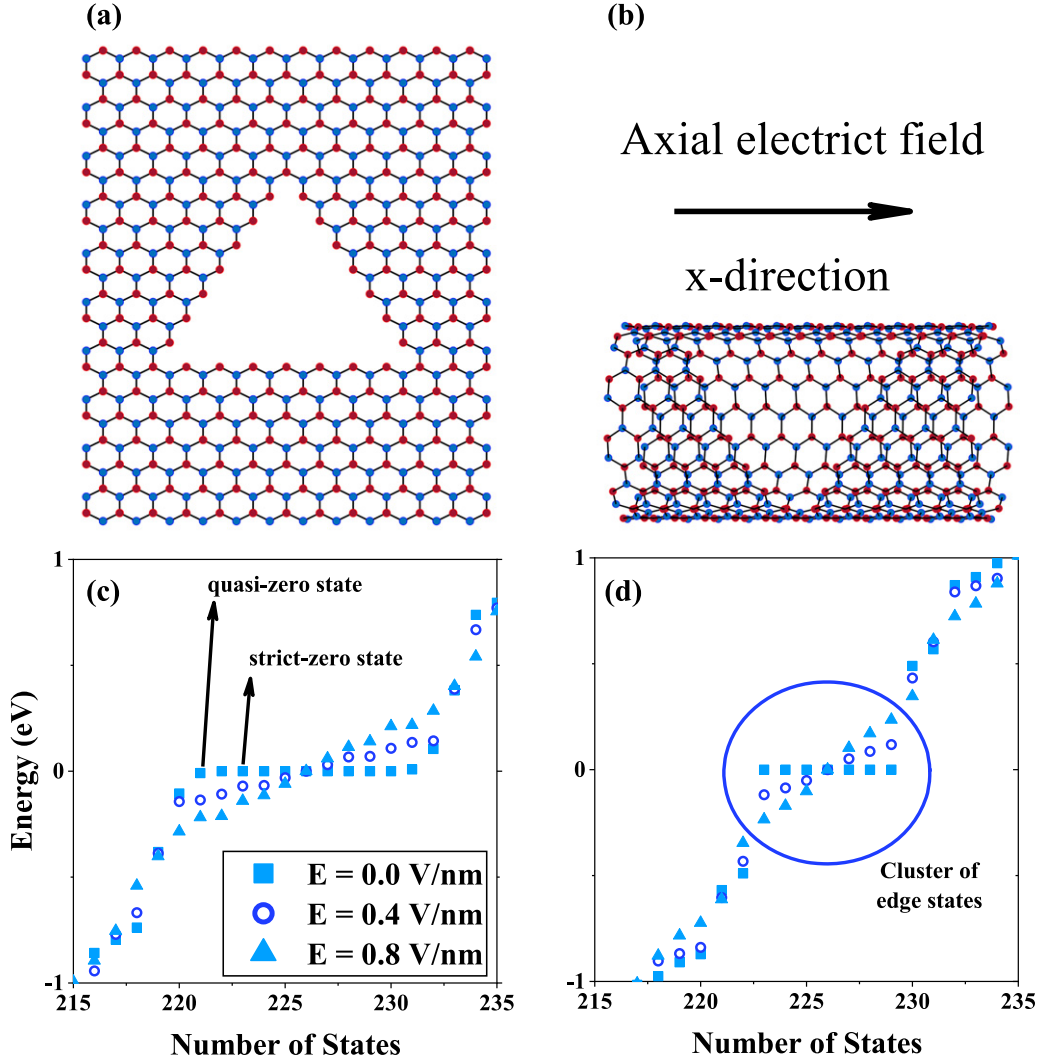
Figure 1. Single-particle spectra and atomic structure. (a) Atomic structure of the graphene sheet with a triangle vacancy, and (b) rolled-up a graphene sheet as a carbon nanotube with the exact vacancy. (c) Single-particle energy spectrum of the graphene sheet, and (d) its counterpart as a carbon nanotube, both in the presence of an axial electric field. Degenerate states are shown in a solid square. The Fermi energy is set to zero.

$$H' = U\sum_i n_i{\uparrow}n_i{\downarrow}, \qquad (4)$$

The parameter U is defining the magnitude of the Coulomb repulsion. $n_{i\sigma} = c^\dagger_{i\sigma}c_{i\sigma}$ is the local density of electrons with spin σ at site i. In this model, two electrons interact only if they occupy the p_z atomic orbital of the same atom. Whereas, the exact solutions are unavailable from the computational point of view. Therefore, the mean-field Hamiltonian can be written as the sum of a Hamiltonian for a spin up, a Hamiltonian for a spin down and a constant as follows:

$$H_{MF} = U\sum_i (n_{i\uparrow}\langle n_{i\downarrow}\rangle + \langle n_{i\uparrow}\rangle n_{i\downarrow} - \langle n_{i\uparrow}\rangle\langle n_{i\downarrow}\rangle), \qquad (5)$$

In this case, the Hamiltonian reduces to one particle problem, and there are a couple of advantages to name. First, the enormous Hilbert space is reduced to the size of the system. Second, the $SU(2)$ symmetry is broken. Finally, the mean-field approximation is closer to an exact solution at a small U [33]. From the computational point of view, the electron–electron

interactions term affects only on diagonal matrix elements of the Hamiltonian and the spin-up and spin-down depends on the unknown expectation values $\langle n_{i\uparrow}\rangle$ and $\langle n_{i\downarrow}\rangle$, respectively. Through a self-consistent procedure starting from an initial condition for average spin-resolved densities $\langle n_{i\sigma}\rangle$ which can be chosen randomly. Diagonalization and computation of the updated spin densities is then repeated iteratively until the values of $\langle n_{i\sigma}\rangle$ are converged. Such a method has been used successfully in the theoretical study of similar graphitic systems, as reported in the literature [6, 29, 34, 35]. Recently, the single-orbital Hubbard model applied to the punctured carbon nanotube in order to study the electronic and transport properties [36].

3. Results and discussions

3.1. Tight-binding model results

In order to assess our theoretical considerations, we first start the development of the tight-binding energy spectrum of
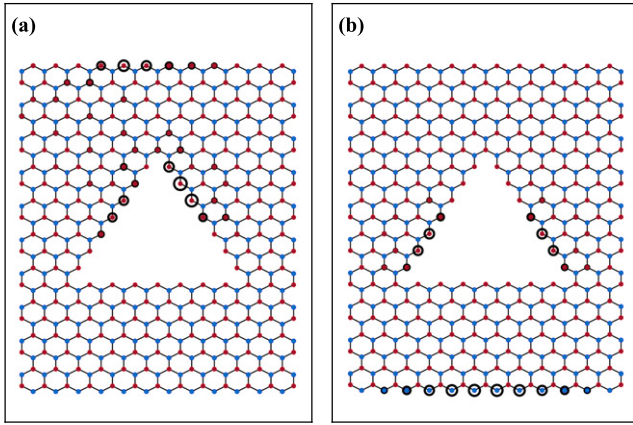
Figure 2. Electronic probability distribution for edge states. (a) An example of wave function in the cluster of strict zero-energy, and (b) in the non-strict zero-energy states in the graphene sheet.

the graphene sheet and its counterpart carbon nanotube. The single-particle spectrum of a nearest-neighbor tight-binding model exhibits electron-hole symmetry due to the bipartite lattice in both structures. The imbalance in sublattices leads to degenerate zero-energy cluster states near the Fermi energy. These zero-energy states are mainly localized at the edges, whereas; the others are extended states. The most striking difference between the energy spectrum of the graphene sheet and its counterpart as a carbon nanotube reflects in the cluster of zero-energy states in both structures. In the case of the graphene sheet with a triangle punctured vacancy, there are 11 zero-energy states available. There are 7 strict zero-energy states due to the imbalance between carbon atoms in sublattice A and B; also, 4 quasi-zero energy states as a result of the ordinary compensated rectangular graphene sheet. These strict zero-energy states are sublattice polarized which means their corresponding wave functions normally widespread on one sublattice, whereas the quasi-zero energy states distributed on different sublattices. Accordingly, the strict zero states wave functions reside in both triangle edges and upper rectangle edge figure 2(a). However, the wave function of quasi-zero energy states is a hybridization of triangle edges and bottom edge of the rectangle graphene sheet figure 2(b). On the other hand, in the case of carbon nanotube, the strict states are exactly as a result of triangle vacancy edges, which makes the imbalance between sublattices.

If we change the coordinate of the triangle vacancy vertically, the probability distributions of electrons for single orbital wavefunctions may vary in the graphene sheet. While this movement through circumferential of the carbon nanotube does not affect electronic probability distribution. Next, when a relatively small electric field is applied to both structures, the cluster zero-energy states are not degenerate anymore in resemblance to the Stark effect [37–39]. And the energy difference between two consecutive energy levels increases almost linearly with the strength of the electric field. The higher electric field strength, the more increase in energy levels figures 1(c) and (d).

3.2. Mean-field Hubbard model results

A simple model which is used for studying magnetic properties of sp^2 carbon allotrope is the single-orbital mean-field Hubbard model. This computational approach is executed in a large number of computer codes. Additionally, this model allows a simple understanding of the many-body systems at the nanoscale and captures the low-energy physics of graphene nanoislands [29].

Self-consistent solution provides the spin densities

$$M_i = \frac{\langle n_{i\uparrow}\rangle - \langle n_{i\downarrow}\rangle}{2} \tag{6}$$

at each atom i and the total spin of the system $S = \sum_i M_i$. For both structures, the average spin densities and local magnetic moments depend merely on the dimensionless parameter U/t. The magnitude parameter U/t may be computed from DFT calculations through some approximations such as the gradient corrected functional PBE, and the local-density approximation (LSDA) [40, 41]. The range of meaningful magnitude is $U/t \sim 1.0$–1.3. In this work a value of $U/t = 1.06$ will be used.

When we add on-site electron–electron interactions to the tight-binding Hamiltonian, we can see the cluster of edge states split into the two sets of different eigenvalues, which each indicates spin up and spin down energy eigenvalues. Each spin-resolved state could be populated by one electron. There is a cluster of $N_A - N_B$ states (e.g., spin-up states) which their energies are lower than the energy of the first state in mentioned cluster with oppositely oriented spins. That is, populating these states at half-filling can be considered as a single-atom Hund's rule figures 3(a) and (e). In the absence of an axial electric field, the maximum total spin of the ground state for both structures is $S = 3.5$. This result is in agreement with the prediction of Lieb's theorem for a bipartite system at half-filling [30].

Spin-resolved energy spectra for both graphene sheet and its counterpart nanotube are shown in figures 3(e) and (a). The energy spreading for such a spin-resolved state is denoted by Δ_D. Figure 4(a) shows the U dependence of energy spreading for both structures. We see that, in the case of the nanotube, the energy spreading is more than the graphene sheet as the strength of Coulomb repulsion increase, and thus the slope of the cluster edge states in nanotube is higher than the graphene sheet due to the rolling operation in nanotube. This rolling action creates circumferential confinement, which led more electrons to move through the entire system, whereas, in the graphene sheet, there is not such confinement. Also, the electronic states demonstrate the highest occupied and lowest unoccupied molecular orbitals (HOMOs–LUMOs). The higher (lower) Δ_D, the more (less) HOMO–LUMO gap in both structures. The position of the triangle vacancy in the graphene sheet is essential. However, this position for a rolled-up graphene sheet as a carbon nanotube is unimportant. Every time the coordinate of the triangle vacancy changes upward (GNR+) or downward (GNR−) in the graphene sheet, the slope of the energy spreading for cluster edge states is still less than the nanotube. Eventually, the energy gap of the nanotube
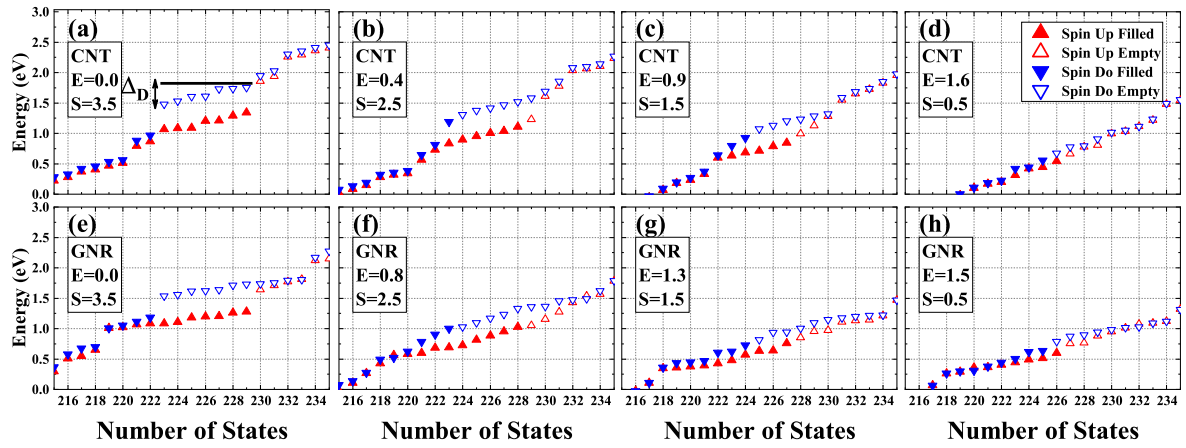
Figure 3. Ground state spin-resolved energy levels obtained through the mean-field Hubbard model calculations for both finite graphene sheet and its counterpart as a carbon nanotube. In the absence of electric field, the ground-state spin is $S = 3.5$ (a), at $E = 0.4$ V nm^{-1} the ground-state spin is $S = 2.5$ (b), at $E = 0.9$ V nm^{-1} the ground-state spin is $S = 1.5$ (c), and finally at $E = 1.6$ the ground-state spin is $S = 0.5$ (d) for carbon nanotube. Likewise for the graphene sheet in the absence of electric field the ground-state spin is $S = 3.5$ (e), at $E = 0.8$ V nm^{-1} the ground-state spin is $S = 2.5$ (f), at $E = 1.3$ V nm^{-1} the ground-state spin is $S = 1.5$ (g), and at $E = 1.5$ V nm^{-1} the ground-state spin is $S = 0.5$. We assume Coulomb repulsion ($U/t = 1.06$). Filled (empty) symbols indicate filled (empty) states, and also up (down) arrows represents up (down) spin.
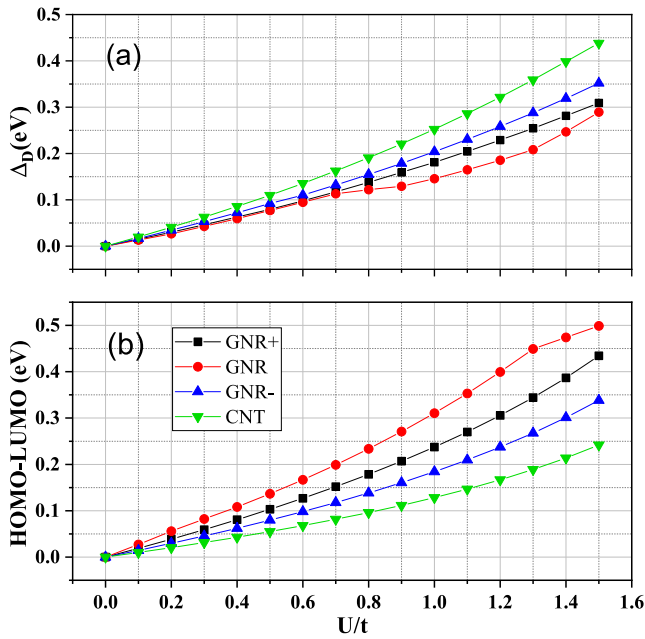

Figure 4. (a) Energy speared for spin-resolved, and (b) the variation of HOMO–LUMO energy gap as a function of Coulomb strength for both graphene sheet and carbon nanotube. $\pm$ symbols for the graphene sheet shows the shift of triangle vacancy upward and downward respectively.

Figure 5. Local spin densities for (a) carbon nanotube at $E = 0.0$ V nm^{-1} with the ground-state spin $S = 3.5$, and (b) at $E = 1.6$ V nm^{-1} with the ground-state spin $S = 0.5$. Besides, local spin-densities for (c) graphene sheet at $E = 0.0$ V nm^{-1} with the ground-state spin $S = 3.5$, and (d) at $E = 1.5$ V nm^{-1} with the ground-state spin $S = 0.5$.

is less than two different situations of the graphene sheet, as illustrated in figure 4(b). Comparing the figures 3(a) and (e) with results displayed in figure 4, one can conclude that the evolution in the electronic structure of the carbon nanotube is more sensitive to the Coulomb repulsion compared to the graphene sheet.

Local magnetic moments of the triangle edges in carbon nanotube are in the same directions. Furthermore, the triangle edges with the upper edge of the rectangular graphene sheet
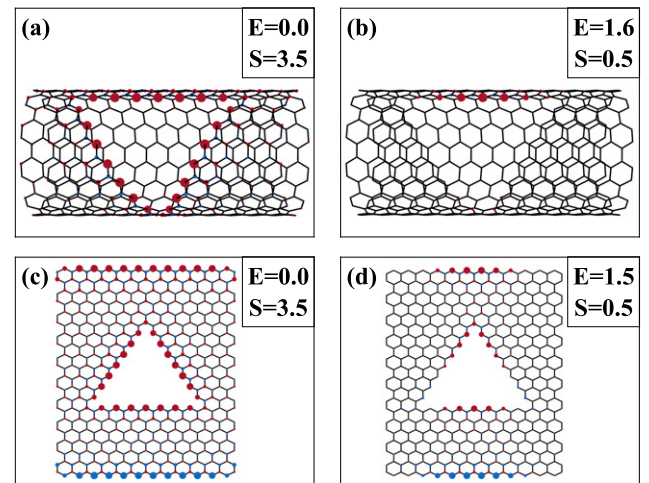
are also in the same directions and represent spin-up densities. These edges are from one sublattice, while the lower rectangular edge of the graphene sheet is in the opposite direction and expresses spin-down densities, as shown in figures 5(a) and (c). The radius of each circle is proportional to the magnitude of density on each site.

Now we are in a position to turn on the axial electric field. As shown in figure 1, we consider the electric field distribution along the mentioned axis for both structures. Electric field increases the energy dispersion of edge states while the spin-resolved extended states tend to be degenerate, as shown in figures 3(b)–(d) for carbon nanotube and figures 3(f)–(h) for
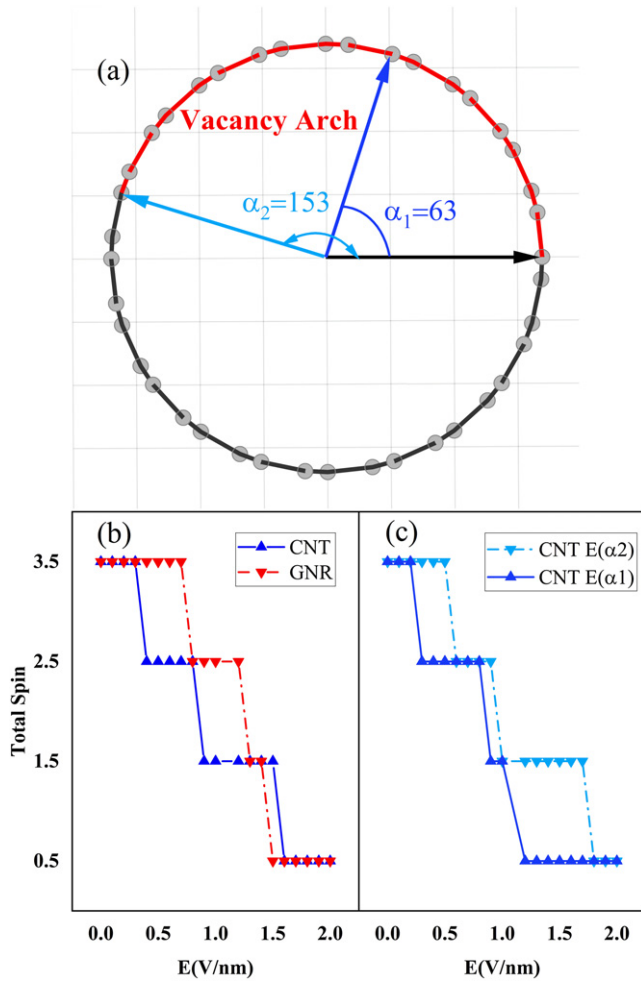
Figure 6. In plane view of the carbon nanotube. Arch of the triangle vacancy illustrated by red. Two critical azimuthal directions shown by α_1 and α_2. (b) Total spin of the both graphene sheet and its counterpart carbon nanotube as a rolled-up graphene sheet as a function of an axial electric field. (c) Total spin of the carbon nanotube at two different directions as a function of perpendicular electric field to the axis.

computational results show that the total spin of the graphene sheet is more robust to depolarize than the total spin of carbon nanotube, stating more sensitivity to the electric field in carbon nanotube compared to the graphene sheet because of the circumferential confinement where exist in carbon nanotube structure which allows more hopping through the whole system.

Finally, a few words have to be said about applying an electric field perpendicular to the axis. For practical applications, we usually use the top or back gate to control the electron or spins. Hence, we consider an electric field perpendicular to the axis to understand how this electric field affects the spin depolarization in carbon nanotube. Due to the asymmetry that the triangle vacancy imposes to the structure, there are two critical azimuthal directions in our selected structure, as it is illustrated in figure 6(a). By applying the perpendicular electric field to the axis at $\alpha_1 = 63$ degree, the total spin of the carbon nanotube decreases to $S = 2.5$ with electric field strength $E = 0.3\,\text{V}\,\text{nm}^{-1}$. In contrast, the first spin depolarization happens in carbon nanotube at $\alpha_2 = 153$ degree with $E = 0.6\,\text{V}\,\text{nm}^{-1}$, which is due to different on-site energies in two different directions. Furthermore, by increasing the strength of the electric field to $E = 1.1\,\text{V}\,\text{nm}^{-1}$ and $E = 1.2\,\text{V}\,\text{nm}^{-1}$, we have found that the total spin of the system decrease to $S = 1.5$ and 0.5 at α_1, respectively. Besides, we have spotted that at α_2, the total spin of the system decreases to $S = 1.5$ and 0.5 at $E = 1.1\,\text{V}\,\text{nm}^{-1}$ and $E = 1.8\,\text{V}\,\text{nm}^{-1}$ as it is clear in figure 6(c).

4. Conclusion

To sum up, by using tight-binding Hamiltonian in combination with the one-orbital Hubbard model at the mean-field approximation, we have compared the magnetic properties, such as spin-resolved edge states, spin depolarization, and the evolution of HOMO–LUMO gaps of the finite graphene sheet and it is counterpart single-walled carbon nanotube as a rolled-up graphene sheet in the presence of a triangle vacancy and an axial electric field. Our results show that the magnetic properties generally depend on the edge states in both structures. By diagonalizing the tight-binding term, we have seen that there is a cluster of 11 edge states, which, 7 out of 11, are strict zero-energy states in the case of graphene sheet as a result of a triangle punctured vacancy. These strict zero states wave functions simultaneously distributed on the edges of the triangle and one zigzag edge of the rectangle graphene sheet. However, the wave functions of the other 4 quasi zero-energy states concentrate on triangle edges and the opposite zigzag edge of the rectangle graphene sheet. Also, there exist 7 strict zero-energy states in the case of carbon nanotube due to the imbalance between sublattice A and B. By adding the single-orbital Hubbard term to the mentioned tight-binding Hamiltonian, we have observed the spin-resolved edge states may happen for both structures and represent spin-up and -down energy levels. Moreover, electron–electron interaction opens a spin gap between the edge states. By increasing an axial electric field, we have spotted that the slope of the cluster edge

graphene sheet. By increasing the electric field, the magnetic moment on each edge atom remains almost unchanged below a crucial value E. The maximum spin-polarized ground state of both structures will be demolished, and spin depolarization may be taking place above a crucial value E (see figure 3). Since the electric field increased to $0.4\,\text{V}\,\text{nm}^{-1}$ in carbon nanotube, the lowest unoccupied state in spin-down lies below the highest occupied state in spin-up; thus, the total spin of the system decreases to 2.5. While in the case of graphene sheet, spin depolarization may occur at $E = 0.8\,\text{V}\,\text{nm}^{-1}$. When the electric field increases to 0.9 or $1.6\,\text{V}\,\text{nm}^{-1}$, the total spin of the carbon nanotube decrease to 1.5 or 0.5, respectively, due to the fewer edge atoms carrying magnetic moments. But, in the graphene sheet, the total spin of the system decreases to 1.5 or 0.5 at $E = 1.3$ or $1.5\,\text{V}\,\text{nm}^{-1}$, respectively. This result demonstrates the fact that carbon nanotube is more sensitive than the graphene sheet at low electric fields. On the other hand, both structures have almost similar spin depolarization at the high electric field. As illustrated in figures 5(b), (d) and 6(b). Our

states in nanotube is higher than the graphene sheet because of the rolling action in nanotube, which creates circumferential confinement. We observed spin-depolarization might occur in nanotube at $E = 0.4$ V nm^{-1}, while in the case of the graphene sheet, it happens at $E = 0.8$ V nm^{-1}. This indicates that carbon nanotube is more sensitive than the graphene sheet at low electric fields. Moreover, both structures have almost similar spin depolarization at the high electric fields.

Acknowledgment

ORCID iDs

A Ghasemifard https://orcid.org/0000-0003-0059-3814
E Faizabadi https://orcid.org/0000-0002-9622-1232

References

[1] Terrones M, Botello-Méndez A R, Campos-Delgado J, López-Urías F, Vega-Cantú Y I, Rodríguez-Macías F J, Elías A L, Munoz-Sandoval E, Cano-Márquez A G, Charlier J C *et al* 2010 Graphene and graphite nanoribbons: morphology, properties, synthesis, defects and applications *Nano Today* **5** 351–72

[2] Nakada K, Fujita M, Dresselhaus G and Dresselhaus M S 1996 Edge state in graphene ribbons: nanometer size effect and edge shape dependence *Phys. Rev.* B **54** 17954

[3] Brey L and Fertig H 2006 Electronic states of graphene nanoribbons studied with the Dirac equation *Phys. Rev.* B **73** 235411

[4] Castro E V, Peres N, dos Santos J L, Neto A C and Guinea F 2008 Localized states at zigzag edges of bilayer graphene *Phys. Rev. Lett.* **100** 026802

[5] Yazyev O V 2010 Emergence of magnetism in graphene materials and nanostructures *Rep. Prog. Phys.* **73** 056501

[6] Sharifian M, Hoseini S and Faizabadi E 2019 Ground state magnetic properties in AA-stacking bilayer graphene quantum dots using Lieb's theorem *J. Magn. Magn. Mater.* **477** 427–33

[7] Jørgensen H I, Grove-Rasmussen K, Wang K Y, Blackburn A, Flensberg K, Lindelof P E and Williams D 2008 Singlet–triplet physics and shell filling in carbon nanotube double quantum dots *Nat. Phys.* **4** 536–9

[8] Iijima S 1991 Helical microtubules of graphitic carbon *Nature* **354** 56

[9] Tans S J, Verschueren A R and Dekker C 1998 Room-temperature transistor based on a single carbon nanotube *Nature* **393** 49

[10] Ebbesen T, Lezec H, Hiura H, Bennett J, Ghaemi H and Thio T 1996 Electrical conductivity of individual carbon nanotubes *Nature* **382** 54

[11] Sanvito S, Kwon Y K, Tománek D and Lambert C J 2000 Fractional quantum conductance in carbon nanotubes *Phys. Rev. Lett.* **84** 1974

[12] Shea H, Martel R and Avouris P 2000 Electrical transport in rings of single-wall nanotubes: one-dimensional localization *Phys. Rev. Lett.* **84** 4441

[13] Shahrjerdi D, Franklin A D, Oida S, Tulevski G S, Han S J, Hannon J B and Haensch W 2011 High device yield carbon nanotube NFETs for high-performance logic applications *2011 Int. Electron Devices Meeting* (IEEE) pp 3–23

[14] Chandra B, Park H, Maarouf A, Martyna G J and Tulevski G S 2011 Carbon nanotube thin film transistors on flexible substrates *Appl. Phys. Lett.* **99** 072110

[15] Han S J, Chang J, Franklin A D, Bol A A, Loesing R, Guo D, Tulevski G S, Haensch W and Chen Z 2010 Wafer scale fabrication of carbon nanotube FETs with embedded poly-gates *2010 Int. Electron Devices Meeting* (IEEE) pp 1–9

[16] Franklin A D, Koswatta S O, Farmer D, Tulevski G S, Smith J T, Miyazoe H and Haensch W 2012 Scalable and fully self-aligned n-type carbon nanotube transistors with gate-all-around *2012 Int. Electron Devices Meeting* (IEEE) pp 4–5

[17] Franklin A D, Luisier M, Han S J, Tulevski G, Breslin C M, Gignac L, Lundstrom M S and Haensch W 2012 Sub-10 nm carbon nanotube transistor *Nano Lett.* **12** 758–62

[18] Franklin A D, Tulevski G S, Han S J, Shahrjerdi D, Cao Q, Chen H Y, Wong H S P and Haensch W 2012 Variability in carbon nanotube transistors: improving device-to-device consistency *ACS Nano* **6** 1109–15

[19] Cao Q, Han S j, Tulevski G S, Zhu Y, Lu D D and Haensch W 2013 Arrays of single-walled carbon nanotubes with full surface coverage for high-performance electronics *Nat. Nanotechnol.* **8** 180

[20] Han S J, Oida S, Park H, Hannon J B, Tulevski G S and Haensch W 2013 Carbon nanotube complementary logic based on Erbium contacts and self-assembled high purity solution tubes *2013 IEEE Int. Electron Devices Meeting* (IEEE) pp 8–19

[21] Tulevski G S, Franklin A D, Frank D, Lobez J M, Cao Q, Park H, Afzali A, Han S J, Hannon J B and Haensch W 2014 Toward high-performance digital logic technology with carbon nanotubes *ACS Nano* **8** 8730–45

[22] Hu Z, Tulevski G S, Hannon J B, Afzali A, Liehr M and Park H 2015 Variability and reliability analysis in self-assembled multichannel carbon nanotube field-effect transistors *Appl. Phys. Lett.* **106** 243106

[23] Tang J, Cao Q, Farmer D B, Tulevski G and Han S J 2016 Carbon nanotube complementary logic with low-temperature processed end-bonded metal contacts *2016 IEEE Int. Electron Devices Meeting* (*IEDM*) (IEEE) pp 1–5

[24] Das R, Shahnavaz Z, Ali M E, Islam M M and Hamid S B A 2016 Can we optimize arc discharge and laser ablation for well-controlled carbon nanotube synthesis? *Nanoscale Res. Lett.* **11** 510

[25] Sari A H, Khazali A and Parhizgar S S 2018 Synthesis and characterization of long-CNTs by electrical arc discharge in deionized water and NaCl solution *Int. Nano Lett.* **8** 19–23

[26] Bardecker J A, Afzali A, Tulevski G S, Graham T, Hannon J B and Jen A K Y 2012 UV-sensitive self-assembled monolayer photoresist for the selective deposition of carbon nanotubes *Chem. Mater.* **24** 2017–21

[27] Hu Z, Hannon J B, Park H, Han S J, Tulevski G S, Afzali A and Liehr M 2017 Photo-chemically directed self-assembly of carbon nanotubes on surfaces (arXiv:1704.01230)

[28] Park H, Afzali A, Han S J, Tulevski G S, Franklin A D, Tersoff J, Hannon J B and Haensch W 2012 High-density integration of carbon nanotubes via chemical self-assembly *Nat. Nanotechnol.* **7** 787

[29] Fernández-Rossier J and Palacios J J 2007 Magnetism in graphene nanoislands *Phys. Rev. Lett.* **99** 177204

[30] Lieb E H 1989 Two theorems on the Hubbard model *Phys. Rev. Lett.* **62** 1201

[31] Ruffieux P, Wang S, Yang B, Sánchez-Sánchez C, Liu J, Dienel T, Talirz L, Shinde P, Pignedoli C A, Passerone D *et al* 2016 On-surface synthesis of graphene nanoribbons with zigzag edge topology *Nature* **531** 489

[32] Talirz L, Sode H, Cai J, Ruffieux P, Blankenburg S, Jafaar R, Berger R, Feng X, Mullen K, Passerone D *et al* 2013

Termini of bottom-up fabricated graphene nanoribbons *J. Am. Chem. Soc.* **135** 2060–3

[33] Feldner H, Meng Z Y, Honecker A, Cabra D, Wessel S and Assaad F F 2010 Magnetism of finite graphene samples: mean-field theory compared with exact diagonalization and quantum monte carlo simulations *Phys. Rev.* B **81** 115416

[34] Farghadan R and Saffarzadeh A 2014 Electric field control of spin-resolved edge states in graphene quantum nanorings *J. Appl. Phys.* **115** 174310

[35] Ma W L and Li S S 2012 Electric-field-induced spin depolarization in graphene quantum dots *Phys. Rev.* B **86** 045449

[36] dos Santos J C, de Vasconcelos F M, de Aguiar A L, de Alencar Alves T F, Meunier V and Girao E C 2016 Electronic, transport, and magnetic properties of punctured carbon nanotubes *Phys. Rev.* B **94** 224106

[37] Agapito L A, Kioussis N and Kaxiras E 2010 Electric-field control of magnetism in graphene quantum dots: *ab initio* calculations *Phys. Rev.* B **82** 201411

[38] Sahoo S, Kontos T, Furer J, Hoffmann C, Gräber M, Cottet A and Schönenberger C 2005 Electric field control of spin transport *Nat. Phys.* **1** 99–102

[39] Wang K, Blackburn A, Wang H, Wunderlich J and Williams D 2013 Spin and orbital splitting in ferromagnetic contacted single wall carbon nanotube devices *Appl. Phys. Lett.* **102** 093508

[40] Perdew J P, Burke K and Ernzerhof M 1996 Generalized gradient approximation made simple *Phys. Rev. Lett.* **77** 3865

[41] von Barth U and Hedin L 1972 A local exchange-correlation potential for the spin polarized case. i *J. Phys. C: Solid State Phys* **5** 1629